

An Anion Metal–Organic Framework with Lewis Basic Sites-Rich toward Charge-Exclusive Cationic Dyes Separation and Size-Selective Catalytic Reaction

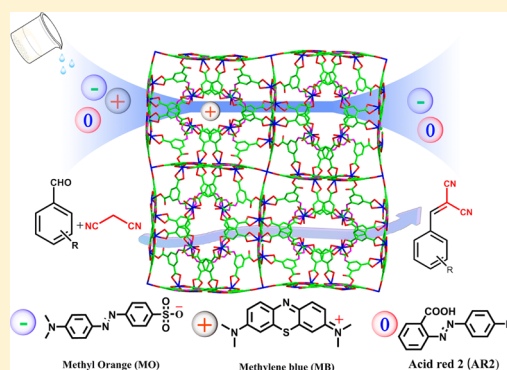
Xu-Sheng Wang,^{†,‡} Jun Liang,[†] Lan Li,[†] Zu-Jin Lin,[†] Partha Pratim Bag,[†] Shui-Ying Gao,[†] Yuan-Biao Huang,^{*,†} and Rong Cao^{*,†}

[†]State Key Laboratory of Structural Chemistry, Fujian Institute of Research on the Structure of Matter, Chinese Academy of Sciences, Fuzhou, Fujian, 350002, China

[‡]University of the Chinese Academy of Sciences, Beijing, 100049, China

Supporting Information

ABSTRACT: Organic dye pollutants become a big headache due to their toxic nature to the environment, and it should be one of the best solutions if we can separate and reuse them. Here, we report the synthesis and characterization of a microporous anion metal–organic framework (MOF) with Lewis basic sites-rich based on TDPAT (2,4,6-tris(3,5-dicarboxyl-phenylamino)-1,3,5-triazine) ligand, **FJI-C2**, which shows high adsorption and separation of cationic dye based on the charge-exclusive effect. Compared to other MOF materials, **FJI-C2** shows the largest adsorption amount of methylene blue (1323 mg/g) at room temperature due to the nature of the anion frameworks and high surface area/pore volume. Furthermore, motivated by the adsorption properties of large guest molecules, we proceeded to investigate the catalytic behaviors of **FJI-C2**, not only because the large pore facilitates the mass transfer of guest molecules but also because the high density of Lewis basic sites can act as effective catalytic sites. As expected, **FJI-C2** exhibits excellent catalytic performance for size-selective Knoevenagel condensation under mild conditions and can be reused several times without a significant decrease of the activity.



INTRODUCTION

Organic dyes, as essential industrial materials, have been widely applied to fibers, such as silk, wool, and nylon.¹ However, they should be removed or recovered to reuse because they are unsustainable and environmentally unfriendly.² So far, to solve the problems, physical, chemical, and biological methods have been developed to treat organic dye wastes.³ Among them, adsorption is considered to be one of the best methods because of its effectiveness and low cost. In this regard, many traditional adsorbents, such as active carbon, zeolites, and polymeric materials, have been used for removing organic dye pollutants.⁴ However, these adsorbents cannot effectively separate target dyes to reuse, which leads to the waste of dyes. Therefore, it is desirable to design and synthesize new adsorbent materials with high adsorption capacity that can separate the dyes effectively.

Porous metal–organic frameworks (MOFs) have been receiving considerable attention in the research areas of gas storage, separations, and catalysis owing to their tunable structure, high surface area/pore volume, and controllable chemical environment.⁵ So far, a handful of MOFs have been used for organic dye adsorption and separation.^{1b,d,e,6} For example, Xu et al. constructed a mesoporous MOF, which can be employed as column-chromatographic fillers for separation of bulk dye molecules.^{6f} Su et al. synthesized a series of pillared-

layer MOFs for separation of rhodamine B and methylene blue.^{6d} Most of the reported MOFs are used to separate organic dyes based on their size exclusion.^{6a–g} However, it is difficult to effectively separate the dyes with similar sizes. Therefore, it is highly desirable to develop porous MOFs to efficiently separate mixed dyes with similar sizes. Porous ionic MOFs bearing a positive/negative charge are potential candidates for selectively separating organic dyes with similar sizes due to the space charge effect between the dyes and MOFs. Recently, Su's group reported a unique cationic MOF as a platform for the highly selective adsorption and separation of anionic organic dyes through an ion-exchange process. Unfortunately, this cationic MOF showed low adsorption capacity (2.6 wt %) and adsorption rate (36 h).^{1h} To the best of our knowledge, rare ionic MOFs have been reported for rapidly separating organic dyes with high capacity.^{1b,h,6i}

In this work, a new microporous negatively charged MOF based on the H₆TDPAT ligand (2,4,6-tris(3,5-dicarboxyl-phenylamino)-1,3,5-triazine), **FJI-C2**, was successfully synthesized by a solvothermal method and structurally characterized by a combination techniques such as single-crystal X-ray

Received: January 6, 2016

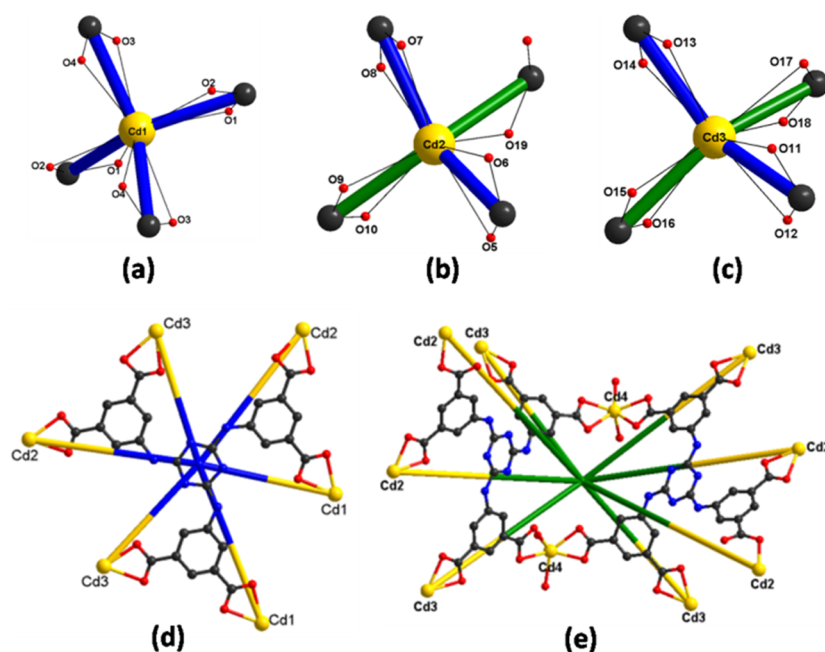


Figure 1. Coordination environments of Cd and TDPAT⁶⁻ in FJI-C2: (a) node1, (b) node2, (c) node3, (d) node4, (e) node5. Color code: Cd, yellow; O, red; N, blue; C, black. For clarity, all hydrogen atoms were omitted.

diffraction (SCXRD), powder X-ray diffraction (PXRD), thermogravimetric analysis (TGA), Fourier transform infrared spectroscopy (FT-IR), ¹H NMR, element analysis, and N₂ sorption. FJI-C2 exhibits highly selective separation and release of cationic dye through an ion-exchange process, which can effectively separate organic dyes with similar sizes. The dye adsorption experiments demonstrate that large reagents are accessible to the active sites in the channels of FJI-C2. It is highlighted that the Lewis basic sites are distributed uniformly over the channels of the FJI-C2, which significantly improves the catalytic activity of the Knoevenagel condensation reactions with size-selectivity.

EXPERIMENTAL SECTION

Materials and Methods. All the reagents and solvents were purchased from commercial sources and used as received, except for H₆TDPAT, which was synthesized according to the literature.^{1g}

Synthesis of H₆TDPAT. 5-Aminoisophthalic acid (0.084 mol), NaOH (0.134 mol), and NaHCO₃ (0.104 mol) were added into 140 mL of H₂O in a round-bottom flask. The mixture was stirred at 0 °C for 30 min; then, 70 mL of 1,4-dioxane containing 0.02 mol of cyanuric chloride was slowly added with constant stirring. The final mixture was refluxed at 110 °C for 24 h. After cooling to room temperature, the solution was adjusted to pH = 1 with concentrated HCl. A white solid (11 g) was collected by centrifugation, washed with distilled water and EtOH, and dried in air. ¹H NMR (*d*₆-DMSO, 400 MHz): δ = 8.12 (3H), 8.47 (6H), 9.68 (3H) ppm.

Synthesis of {Cd_{3.5}(TDPAT)₂[(CH₃)₂NH₂]⁺₅·(H₂O)₂·(H₂O)₂₀ (FJI-C2). CdCl₂ (0.02 mmol), H₆TDPAT (0.01 mmol), and HBF₄ (0.05 mL) were added into a mixed solvent (2 mL, DMF/MeOH = 1:1) in a 10 mL vial. The mixture was ultrasonicated for 20 min and heated at 80 °C for 3 days, and then cooled to room temperature. Colorless rodlike crystals were obtained by filtration, washed with CH₂Cl₂ several times, and dried by vacuum at ambient temperature. The compound is insoluble in common organic solvents such as methanol, ethanol, acetonitrile, acetone, DMSO, and DMF. Colorless rodlike crystals were collected in 79.5% yield based on H₆TDPAT. IR (KBr, cm⁻¹, Figure S1): 3399 (s), 3311 (s), 3196 (s), 3116 (s), 1633 (s), 1535 (vs), 1416 (s), 1371 (vs), 1147 (w), 1113 (w), 1016 (w), 958 (w), 897 (w), 798 (m), 777 (m), 732 (m), 620 (m).

Dye Adsorption and Separation. To evaluate the accessibility of dyes to the voids of the frameworks, both the dyes' charge and size need to be considered. The capture experiments of individual dye were performed on FJI-C2 first. Typically, 10 mg of fresh crystalline samples of FJI-C2 were put in the dye solution (10 mL). The adsorption abilities of FJI-C2 toward those dyes were determined by UV-vis spectroscopy. Afterward, we arranged the organic dyes in two groups. Dyes in the first group have different charges, but similar sizes (methylene blue (MB⁺), methyl orange (MO⁻), acid red 2 (AR2⁰)), whereas dyes in the second group have the same charge, but different sizes (methylene blue (MB⁺), rhodamine 6G (R6G⁺)). Typically, the fresh crystalline samples of FJI-C2 (10 mg) were put in the mixed dyes solutions (10 mL). UV-vis spectra were used to measure the rapid and selective dye adsorption ability of FJI-C2. All the concentration of MB⁺, MO⁻, AR2⁰, and R6G⁺ is 0.03 mmol/L.

The maximum adsorption capacity of MB⁺ was investigated by adding 35 mg of as-synthesized FJI-C2 into of a 10 mmol/L DMF solution (20 mL) for 25 h at room temperature. UV-vis spectra were used to measure the maximum adsorption capacity of methylene blue by FJI-C2.

Dye Release. Dye-releasing experiments were performed on pure DMF and NaCl-containing DMF solution, respectively. UV-vis spectra were used to measure the release ability of FJI-C2.

Knoevenagel Condensation Reaction. A 50 mg portion of FJI-C2 (3 mol % with respect to the amount of benzaldehyde) was added to a mixture of benzaldehyde (or benzaldehyde derivative) (1 mmol) and malononitrile (1.1 mmol) in toluene (5 mL). After the mixture was stirred in a preheated oil bath (35 °C) in air for the appropriate time, the resultant mixture was filtered. The filtrate was analyzed by GC and GC-MS to identify the structure of the target product.

Reusability of FJI-C2 in the Knoevenagel Condensation Reaction. A mixture of FJI-C2 (50 mg), 4-cyanobenzaldehyde (1 mmol), and malononitrile (1.1 mmol) in toluene (5 mL) was stirred at 35 °C in air for 6 h. After reaction, the mixture was filtered, and the filtrate was analyzed by GC. After the reaction, the catalyst was separated by simple centrifugation, and washed with toluene for three times. The recovered catalyst was reused in further reaction under identical conditions to those of the first run with aliquots analyzed by GC.

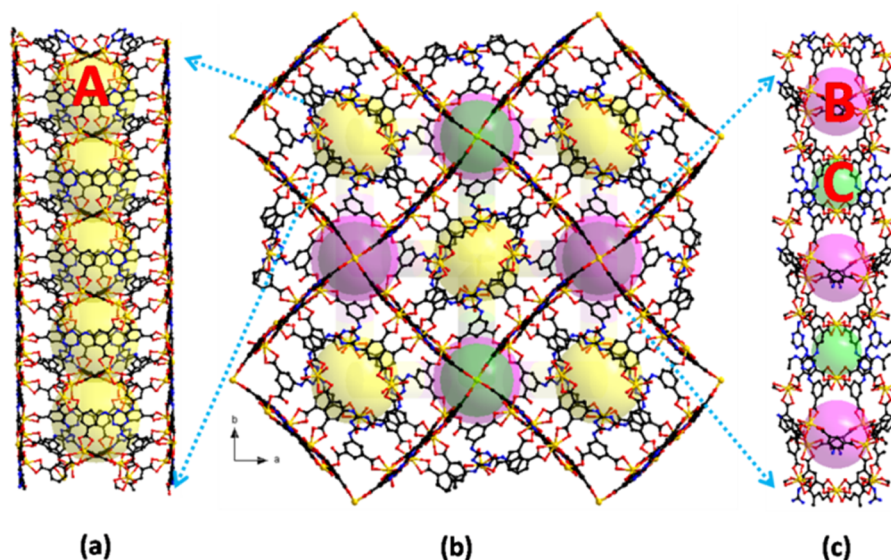


Figure 2. Packing diagram of FJI-C2, showing the 1D opening channels as viewed along the c axis. (a) The channel with A cages along c axis, (b) 3D packing diagram, (c) the distribution of B and C cages along c axis. Color code: Cd, green; O, red; N, blue; C, black; A cage, yellow ball; B cage, pink ball; C cage, green ball. The diameters of cages A, B, and C are 15, 11, and 8 Å, respectively. The size of the 1D opening channels is 12.4×7.1 Å. Both sizes of channels and cages are measured between opposite atoms without taking account of van der Waals radii of the atoms. For clarity, all hydrogen atoms were omitted.

RESULTS AND DISCUSSION

Description of the Crystal Structure. The compound FJI-C2 was obtained by the reaction of H_6TDPAT (H_6L) and $CdCl_2$ in the mixture solvents of DMF/ CH_3OH (1:1, v/v) with a little HBF_4 . The chemical formula of FJI-C2 was confirmed by SCXRD, charge-balance considerations, 1H NMR (Figure S2), TGA (Figure S3), and elemental analysis (EA). Single-crystal X-ray diffraction revealed that FJI-C2 is a 3D anion framework, which crystallizes in the acentric group $P\bar{4}2_1c$ (No. 114) (Table S1). The negative charge is balanced by organic cations ($[(CH_3)_2NH_2]^+$) that are generated in situ upon solvent decomposition during the solvothermal synthesis.^{1c} As shown in Figure 1, the asymmetric unit of FJI-C2 contains three and a half independent Cd(II) (Cd1, Cd2, Cd3, and Cd4) nodes, two TDPAT⁶⁻ (L1 and L2) linkers, and two water molecules. The coordination environment is depicted elaborately in the Supporting Information. The phase purity of the bulk product was confirmed by the powder X-ray diffraction (PXRD) analysis (Figure S8). 1H NMR reveals that only H_2O and $[(CH_3)_2NH_2]^+$ existed in the channel of FJI-C2. The ratio of $[(CH_3)_2NH_2]^+ : TDPAT$ is 2.5:1, which is consistent with the charge-balance calculation (calcd: 2.5:1). The TGA curve reveals a weight loss of 17.82% (calcd: 17.34%) from room temperature to 120 °C, which can be attributed to the loss of uncoordinated water. Thereafter, a weight loss of 11.62% (calcd: 12.82%) to 340 °C prior to decomposition was observed, which corresponds to the loss of $[(CH_3)_2NH_2]^+$ cations and coordinated water. Elemental analysis (%) calcd for $\{Cd_{3.5}(TDPAT)_2[(CH_3)_2NH_2^+]_5 \cdot (H_2O)_2\} \cdot (H_2O)_{20}$: C 32.96%, H 5.07%, N 10.51%; found: C 36.95%, H 5.20%, N 11.46%.

To improve the understanding of the framework, a topology method was applied to analyze FJI-C2 using the nodes mentioned above. As shown in Figure S4, the nodes are connected through metal–carboxylate bonds and it reveals an unprecedented (4,4,4,6,8)-connected net with the Schläfli symbol $\{4^4.6^{10}.8\}_2\{4^4.6^{12}.8^{12}\}\{4^4.6^2\}_4\{4^6\}$. To the best of our

knowledge, this is an extraordinary topology which has not been reported.

Interestingly, large nanotubes with a size of 12.4×7.1 Å are formed by Cd metals and TDPAT linkers viewed in the [110] direction. There are three kinds of microporous cages (cage A, cage B, and cage C) with different sizes in the range of 15, 11, and 8 Å, respectively (Figure 2). The size distribution of FJI-C2 was also simulated by poreblazer v3.0 software developed by Lev Sarkisov in 2012 (Figure S5), which is a little smaller than that measured by X-seed software due to that the van der Waals radii of the atoms is counted.⁷ It is worth noting that those cages are connected with each other throughout the MOF.

The total accessible volume of FJI-C2 is 20201.4 Å³, which corresponds to 69.6% empty volume (29014.5 Å³) by the PLATON calculation. The accessible special surface area can reach 2315 m²/g, which was calculated by poreblazer v3.0 software. However, the N₂ adsorption experiment failed to give an expected result to calculate the surface area, probably because the long-range order structures of the frameworks were lost under activation at high vacuum, which often happens in some highly porous MOFs.^{1g,8} The unique structural features of FJI-C2 (large aperture, pore volume and special surface area, anion framework with counter cations, high density of Lewis basic sites) indicate that it has the potential applications in dye separation based on size-/charge-exclusion and size-selective catalytic reaction.

Dye Adsorption and Separation Properties. On the basis of the large aperture in the anion framework of FJI-C2, the investigation of dye capture and separation in solution seems to be promising to explore the porosity and its potential application. To evaluate the accessibility of dyes to the voids of the frameworks, both dyes' charge and size need to be considered. Thus, we arranged the organic dyes in two groups. Dyes in the first group (methylene blue (MB^+), methyl orange (MO^-), acid red 2 ($AR2^0$)) have similar sizes with different charges, whereas another group of dyes (methylene blue (MB^+), rhodamine 6G ($R6G^+$)) have the same charge, but

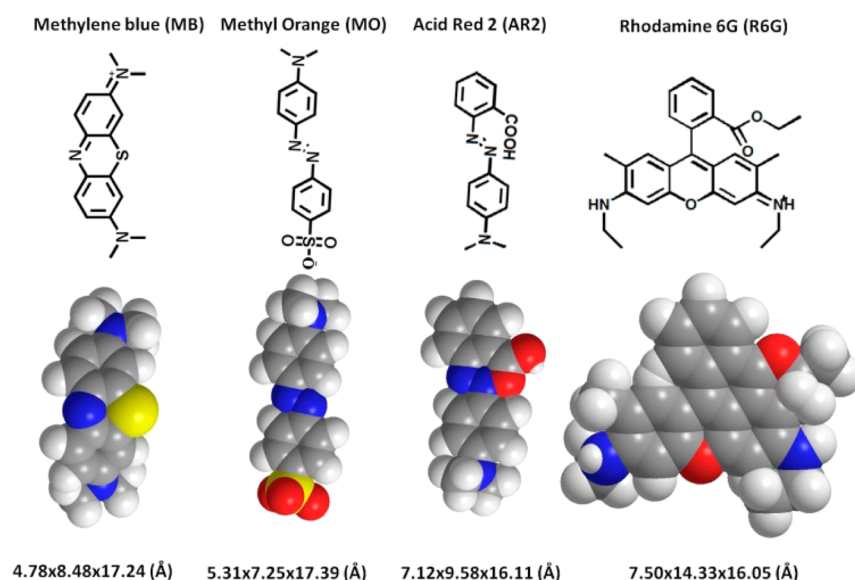


Figure 3. Molecular structures of the organic dyes with a similar backbone used in this study.

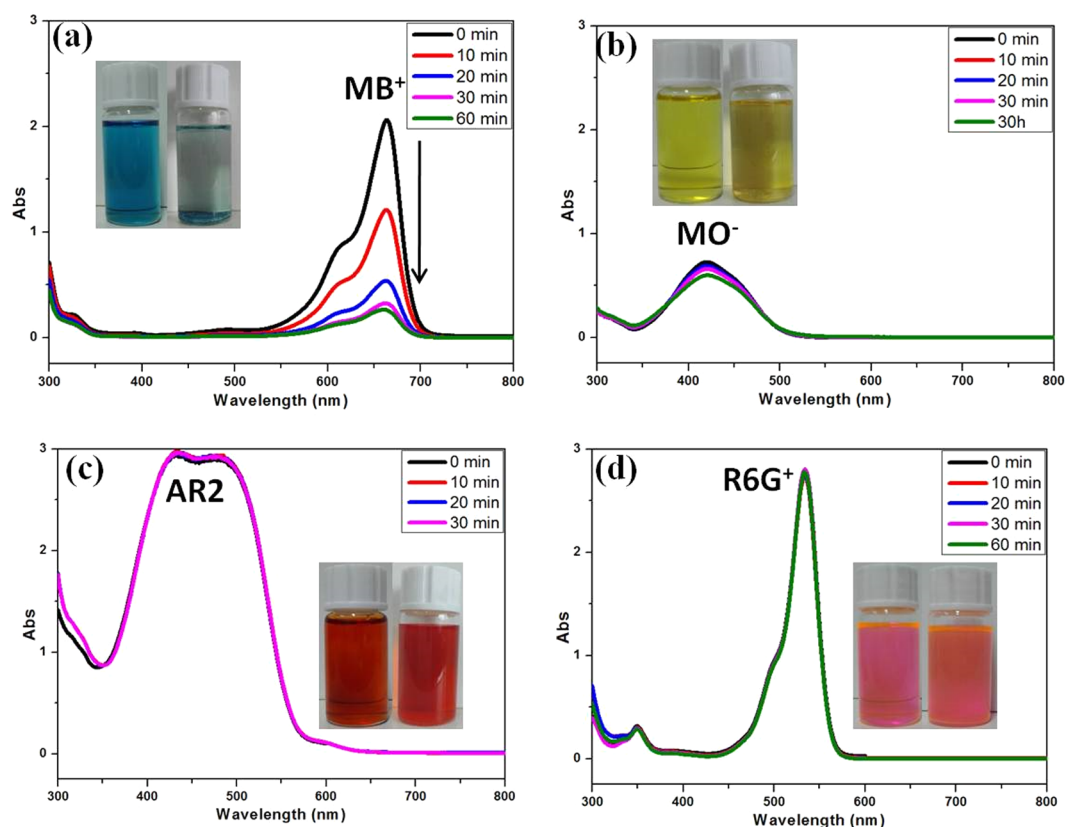


Figure 4. UV-vis absorption curves of MB^+ (a), MO^- (b), AR2^0 (c), R6G^+ (d). The inserted photographs show the colors of the solutions before (left) and after (right) organic dyes adsorption.

different sizes. The dimensions of organic dyes with different charges and sizes are listed in Figure 3.

The capture experiments of individual dye were performed using FJI-C2. Typically, the fresh crystalline sample of FJI-C2 was immersed into the dye solution. The adsorption abilities of FJI-C2 toward these dyes were determined by UV-vis spectroscopy. As shown in Figure 4, nearly all the cationic MB^+ can be captured in 1 h. This can be further seen from the color change of solution in which the blue gradually became

colorless. Moreover, compared to other absorbents using a few days,^{2,5,8} the absorption rate of MB^+ by FJI-C2 was really fast, and 90% of dye molecules can be adsorbed in 1 h. The high adsorption rate is attributed to the large size of the cage windows ($12.4 \times 7.1 \text{ \AA}$) and negative charge framework. Notably, the FJI-C2 has the highest adsorption amount of MB^+ (1323 mg/g at room temperature) among all the other MOF materials at higher MB^+ concentration. What's more, the adsorption capacity is also higher than that of most of the other

absorbents, such as active carbon, graphene oxide sponge, and tea waste (Figure S6 and Table S3), monitored by UV-vis spectroscopy.^{2b,4b,9} On the contrary, the anionic MO^- and neutral AR2^0 cannot be effectively absorbed due to the negative charge framework of FJI-C2. Besides, the cationic R6G^+ was also excluded by FJI-C2 because of the larger size than that of the aperture of the framework. The selective absorption of cationic dyes by FJI-C2 could be attributed to the anionic framework, in which the $[(\text{CH}_3)_2\text{NH}_2]^+$ cations can be exchanged with cationic dyes. To confirm this mechanism, dye-releasing experiments were performed in pure DMF and NaCl-containing DMF solution, respectively. UV-vis spectroscopy in Figure 5 shows that the intensity of MB^+ decreases

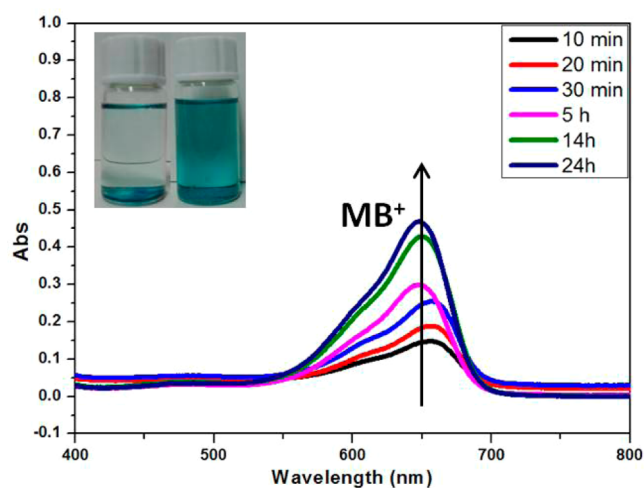


Figure 5. UV-vis absorption curves of MB^+ release from $\text{MB}^+\text{@FJI-C2}$ in NaCl-containing DMF solution.

along with the time. At the same time, the colorless solution gradually changes to blue. The above results indicated that the dye molecules release from the pore of $\text{MB}^+\text{@FJI-C2}$ in the presence of Na^+ cations. In contrast, the dye molecules are difficult to release in pure DMF, which can be indicated by UV-vis spectroscopy in Figure S7. In addition, the PXRD of $\text{MB}^+\text{@FJI-C2}$ and $\text{MB}^+\text{-released@FJI-C2}$ show the same patterns as the as-synthesized FJI-C2, indicating the stability of crystalline sample FJI-C2 (Figure S8).

The selective adsorption of dye molecules based on charge- or size-exclusion and dye-releasing experiments proved that the MB^+ can enter the voids of FJI-C2. To further check the fact, the color of the crystal inside was observed. Typically, $\text{MB}^+\text{@FJI-C2}$ was washed with DMF several times to remove the MB^+ on the surface of FJI-C2. Then, one rodlike $\text{MB}^+\text{@FJI-C2}$ was selected and cut to check the cross section of $\text{MB}^+\text{@FJI-C2}$. The color of both the inner and the outer parts of $\text{MB}^+\text{@FJI-C2}$ was blue (Figure S9), which indicates that MB^+ molecules have been absorbed inside the voids of FJI-C2.

The separation process based on charge- and size-selectivity is further demonstrated in the solutions containing two different dyes. To exclude the size effect, a mixture of a cationic dye (MB^+) and an anionic dye (MO^-) was chosen because they have opposite charges but with similar small sizes (Figure 6a). A blue solution of MB^+ and an orange solution of MO^- were mixed thoroughly to give a green colored solution. The color of the solution gradually turned orange from green and essentially became to display the color of the pure MO^- after addition of FJI-C2 in 1 h. Meanwhile, the colorless FJI-C2

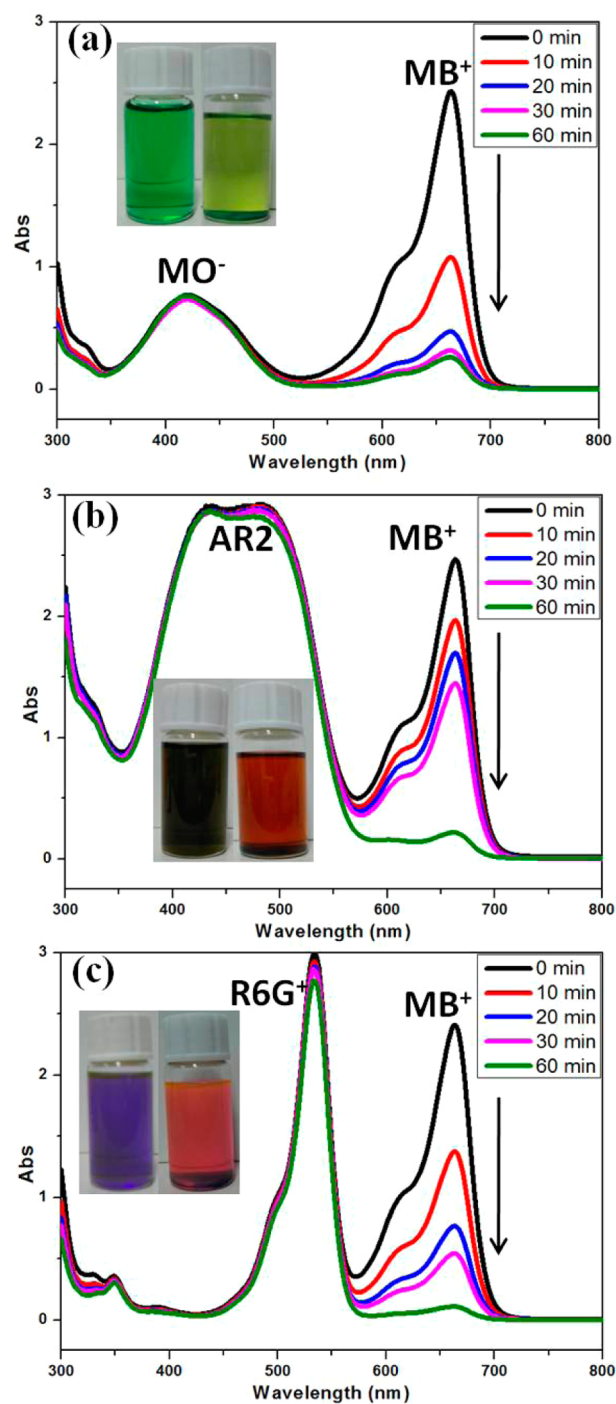


Figure 6. UV-vis absorption curves of MB^+/MO^- (a), $\text{MB}^+/\text{AR2}^0$ (b), $\text{MB}^+/\text{R6G}^+$ (c). The inserted photographs show the colors of the mixed solutions before (left) and after (right) organic dyes absorption.

crystal at the bottom of the vial became blue, which indicated that the cationic dye MB^+ was selectively trapped within the pore. Afterward, the cationic dye (MB^+) and a neutral dye (AR2^0) were chosen as guests based on the similar reason mentioned above (Figure 6b). Next, the FJI-C2 was added to the mixture solution, and the dark brown solution changed to light brown gradually, and to reddish brown almost the same color of AR2^0 . The above observation was also proved by the UV-vis spectroscopy. The result implied that only the cationic

guest could enter FJI-C2, whereas the anionic or neutral one cannot be adsorbed by the anionic framework.

To demonstrate size dependency, the separation of a mixture of MB^+ and R6G^+ was monitored by UV-vis spectroscopy in the presence of FJI-C2 (Figure 6c). MB^+ and R6G^+ were chosen because they have the same charge but with significantly different sizes. The color of the mixture of the blue-colored MB^+ and the red-colored R6G^+ become violet. After the addition of FJI-C2, the color of the solution gradually turned to red color (identical to the pure R6G^+ solution). This observation was supported by UV-vis spectroscopy measurements. Those results indicated that the dyes with small sizes can enter the pore of FJI-C2, while the large one was excluded by the framework.

Catalytic Properties. Motivated by the adsorption properties of large guest molecules, we proceeded to investigate the catalytic behaviors of FJI-C2, not only because the large pore facilitates the mass transfer of guest molecules but also because the high density of Lewis basic sites can act as effective catalytic sites. Knoevenagel condensation reaction catalyzed by base is important for producing of fine chemicals, pharmaceutical products, and perfumes.¹⁰ Considering the easy recovery and reuse property, the development of heterogeneous catalysts is a topic of great interest.^{10,11} Interestingly, the high density of Lewis basic sites is uniformly distributed in the frameworks of FJI-C2, which will facilitate the heterogeneous Knoevenagel condensation reaction. Moreover, the sizes of the substrates and the product 2-benzylidene malononitrile ($3.02 \times 9.63 \times 9.99 \text{ \AA}$) are smaller than the size of channel windows in FJI-C2 ($1.24 \times 0.71 \text{ nm}$), which is favorable for the accessibility of substrates to catalytic active sites inside the framework. For a typical procedure, benzaldehyde was reacted with malononitrile at 35°C in toluene in the presence of the catalyst FJI-C2 (3 mol % with respect to the amount of benzaldehyde). As shown in Figure 7, FJI-C2 gives an 81% yield of 2-benzylidene

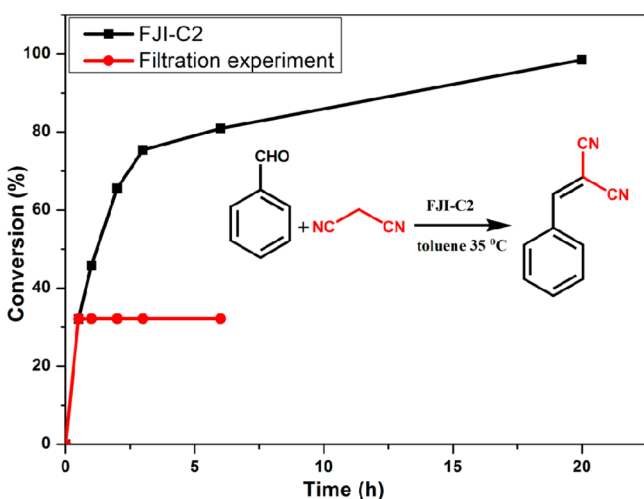


Figure 7. Yield of 2-benzylidenemalononitrile in the Knoevenagel condensation reaction with different reaction times.

malononitrile in 6 h. Nearly full conversion of benzaldehyde was achieved (98.5%) with a prolonged time to 20 h. To check the heterogeneity of FJI-C2 in the Knoevenagel condensation reaction, a filtration experiment was also conducted. After the reaction mixture was stirred for half an hour, removal of the catalyst via filtration resulted in the complete shut down of the

reaction, which verifies the heterogeneous catalysis of FJI-C2. A blank experiment without any catalyst showed that no product was detected by GC, which ensured that FJI-C2 is indeed responsible for the high catalytic activity (Table 1, entry 2).

Table 1. Knoevenagel Condensation Reaction of Malononitrile with Benzaldehyde Derivatives^a

entry	-R	time (h)	yield (%) ^b
1	4-H	6	80.9
2 ^c	4-H	6	0
3 ^d	4-H	6	17.5
4 ^e	4-H	6	0.5
5 ^f	4-H	6	0
6 ^g	4-H	6	0
7	4-CN	6	92.4
8	4-NO ₂	6	91.5
9	4-F	6	76.5
10	4-Cl	6	89.3
11	4-Br	6	82.6
12	4-Ph	6	44.6
13	4-CH ₃	6	74.1
14	2-OCH ₃	6	77.8
15	3-OCH ₃	6	65.0
16	4-OCH ₃	6	42.8

^aReaction conditions: benzaldehyde or benzaldehyde derivatives (1 mmol), malononitrile (1.1 mmol), FJI-C2 (50 mg), toluene (5 mL), at 35°C for 6 h. ^bThe yield was determined by GC and GC-MS. ^cNo catalyst was added. ^dThe desolvated FJI-C2 (50 mg as-synthesized FJI-C2 was dried in 70°C for overnight) was used as catalyst instead of the as-synthesized FJI-C2. ^e H_6TDPAT (50 mg) was used as catalyst instead of FJI-C2. ^f CdCl_2 (10 mg) was used as catalyst instead of FJI-C2. ^gResidual solvent (DMF 20 μL plus H_2O 20 μL) was used as catalyst instead of FJI-C2.

What's more, a very low yield (17.5% in 6 h) was observed when the desolvated FJI-C2 was employed due to collapse of the framework of the desolvated one (Table 1, entry 3). Besides, the ligands H_6TDPAT , CdCl_2 , or residual solvent (DMF and water) was performed, which also resulted in almost no product (Table 1, entries 4–6). Those control experiments clearly imply that the channels of FJI-C2 catalyst play a vital role in the Knoevenagel condensation reaction.

To further study the substrate scope, several benzaldehyde derivatives with malononitrile were performed under the same conditions (Table 1). The electron-deficient benzaldehyde derivatives, such as 4-cyanobenzaldehyde, 4-nitrobenzaldehyde, and 4-halogenobenzaldehyde, gave the corresponding products with higher conversion in the Knoevenagel condensation (Table 1, entries 7–11). On the contrary, the electron-rich benzaldehyde derivatives, such as 4-methylbenzaldehyde, 4-methoxybenzaldehyde, and 4-phenylbenzaldehyde, obtained lower yields of the corresponding products (Table 1, entries 12–16). The high yields of the benzaldehyde derivatives containing electron-withdrawing groups were obtained because nucleophilic addition is the rate-determining step in the Knoevenagel condensation. Notably, 4-chlorobenzaldehyde

Table 2. Knoevenagel Condensation Reaction of Benzaldehyde with Substrates^a

Entry	Product	Size of product (Å)	Time (hours)	Yield (%) ^[b]
1		3.02×9.63×9.99	6	80.9
2		4.89×10.25×13.44	6	1.5
3		7.32×10.81×13.44	6	0
4		7.35×10.93×14.40	6	0

^aReaction conditions: benzaldehyde (1 mmol), substrates (1.1 mmol), FJI-C2 (50 mg), toluene (5 mL), at 35 °C for 6 h. ^bThe yield was determined by GC and GC-MS.

with nearly 90% conversion has the best catalytic performance among 4-halogenobenzaldehyde, mainly due to the synergistic effect by the inductive effect and the conjugation effect. Even though the fluorine groups in benzene rings have the strongest inductive effect, their conjugation effect is also the strongest among halogen groups. The synergistic effect by the inductive effect and the conjugation effect makes the electron-withdrawing property of 4-halogenobenzaldehyde in the order of $-Cl > -Br > -F$; thus, the conversion of 4-halogenobenzaldehyde decreases in the order of the same sequence (Table 1, entries 9–11). Considering that the nitro and cyano functional groups have strong electron-withdrawing ability, as expected, the conversion of the two benzaldehyde derivatives with malononitrile is more than 90% (Table 1, entries 7 and 8). In comparison, the electron-rich benzaldehyde derivatives, such as 4-methylbenzaldehyde and 4-phenylbenzaldehyde, gave the corresponding products with lower than 80% yields (Table 1,

entries 12 and 13). In order to investigate the effect of functional groups in different substituent sites, the *ortho*-, *meta*-, and *para*-methoxybenzaldehyde were selected to react with malononitrile under the same conditions (Table 1, entries 14–16). The substrate *ortho*-methoxybenzaldehyde gave a 77.8% GC yield, whereas *meta*- and *para*-methoxybenzaldehyde afford the corresponding products in 65.0% and 42.8% GC yield, respectively. This phenomenon is ascribed to the existence of the intramolecular hydrogen bonds between the O atom of the methoxy group and the H atom of the formyl group, which leads to that *ortho*-methoxybenzaldehyde can be easily attacked by nucleophiles and gives a higher yield of 2-(2-methoxybenzylidene)-malononitrile.

To further probe whether the Knoevenagel reaction occurred inside the pores or on the surface of the solid catalyst, active methylene substrates of increasing dimensions were tested for the catalyst FJI-C2 (Table 2). In the case of malononitrile, the

conversion of benzaldehyde was 80.9% in 6 h (Table 2, entry 1). As for the even larger cyanoacetic acid ethyl ester, the condensation reaction with benzaldehyde decreased obviously to 1.5% under the same conditions (Table 2, entry 2). With the substrates further increase, for example, *tert*-butyl cyanoacetate or di-*tert*-butyl malonate, the reactions with benzaldehyde did not proceed (Table 2, entries 3 and 4). Since the pore size of FJI-C2 is 1.24×0.71 nm, larger substrates were excluded by FJI-C2, which proves that the reactions occur inside the pores.

Easy separation as well as the deactivation and reusability are the most significant factors for industrial application (Figure 8).

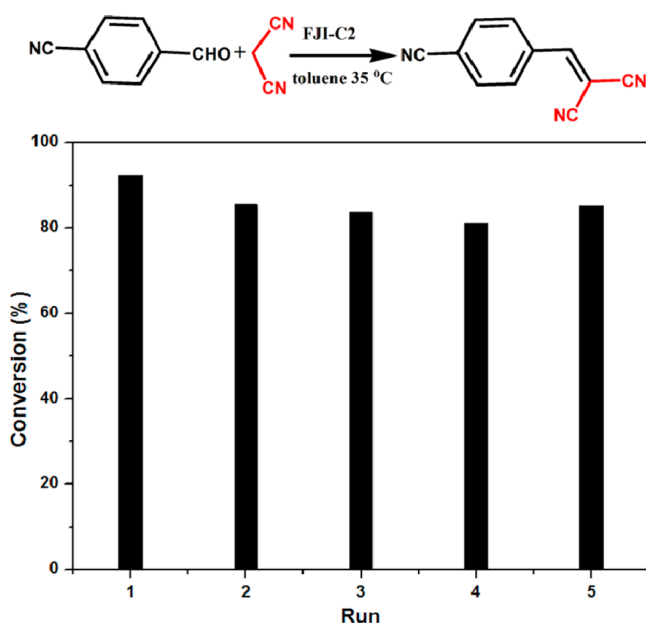


Figure 8. Reusability of FJI-C2. Reaction conditions: 4-cyanobenzaldehyde (1 mmol), malononitrile (1.1 mmol), FJI-C2 (50 mg), toluene (5 mL), at 35 °C for 6 h.

FJI-C2 was, therefore, investigated for recoverability and reusability in the Knoevenagel reaction. The reaction was carried out in toluene at 35 °C using 3 mol % catalysts for 6 h. After the reaction, the catalyst was separated by simple centrifugation, and washed with toluene for three times. The recovered catalyst was reused in further reaction under identical conditions to those of the first run with aliquots analyzed by GC. The results demonstrated that FJI-C2 catalyst could be recovered and reused without a significant decrease in activity. It was observed that more than 80% conversion was still achieved even after five consecutive cycles. At the same time, PXRD shows that the crystallinity of the catalyst was retained after five runs (Figure S8).

CONCLUSIONS

In summary, a new microporous anion metal–organic framework FJI-C2 has been synthesized by employing nitrogen-containing ligands and CdCl_2 under solvothermal conditions. FJI-C2 exhibits highly selective adsorption and separation of cationic dye in DMF solution through an ion-exchange process based on the charge-exclusion effect. Compared to other MOF materials, FJI-C2 has the highest adsorption amount of MB^+ at room temperature. What's more, benefiting from the contribution of high density of Lewis basic sites and uniform pore distribution, FJI-C2 was employed as an

efficient, heterogeneous, reusable catalyst for the size-selective Knoevenagel condensation reaction under mild conditions.

ASSOCIATED CONTENT

Supporting Information

The Supporting Information is available free of charge on the ACS Publications website at DOI: 10.1021/acs.inorgchem.6b00019.

Instruments for characterization, coordination environment of FJI-C2, and some related tables and figures (PDF)

Crystallographic data for FJI-C2 (CIF)

AUTHOR INFORMATION

Corresponding Authors

*E-mail: ybhuang@fjirsm.ac.cn (Y.-B.H.).

*E-mail: rcao@fjirsm.ac.cn. Fax: (+86)-591-63173153. Tel: (+86)-591-63173153 (R.C.).

Author Contributions

All authors have given approval to the final version of the manuscript.

Notes

The authors declare no competing financial interest.

ACKNOWLEDGMENTS

We acknowledge the financial support from the 973 Program (2012CB821705 and 2013CB933200), NSFC (21273238, 21521061, 21331006, and 21303025), the Natural Science Foundation of Fujian Province (2014J05022, 2014J05020) and the Chunmiao Project of Haixi Institute of Chinese Academy of Sciences (CMZX-2014-004) and Youth Innovation Promotion Association, CAS (2014265).

REFERENCES

- (1) (a) Liu, L.; Zhang, X.-N.; Han, Z.-B.; Gao, M.-L.; Cao, X.-M.; Wang, S.-M. *J. Mater. Chem. A* **2015**, *3*, 14157–14164. (b) He, Y.-C.; Yang, J.; Kan, W.-Q.; Zhang, H.-M.; Liu, Y.-Y.; Ma, J.-F. *J. Mater. Chem. A* **2015**, *3*, 1675–1681. (c) Haque, E.; Lo, V.; Minett, A. I.; Harris, A. T.; Church, T. L. *J. Mater. Chem. A* **2014**, *2*, 193–203. (d) Han, Y.; Sheng, S.; Yang, F.; Xie, Y.; Zhao, M.; Li, J.-R. *J. Mater. Chem. A* **2015**, *3*, 12804–12809. (e) Sun, C. Y.; Wang, X. L.; Qin, C.; Jin, J. L.; Su, Z. M.; Huang, P.; Shao, K. Z. *Chem.—Eur. J.* **2013**, *19*, 3639–3645. (f) Qin, J. S.; Zhang, S. R.; Du, D. Y.; Shen, P.; Bao, S. J.; Lan, Y. Q.; Su, Z. M. *Chem.—Eur. J.* **2014**, *20*, 5625–5630. (g) Zhu, Z.; Bai, Y. L.; Zhang, L.; Sun, D.; Fang, J.; Zhu, S. *Chem. Commun.* **2014**, *50*, 14674–14677. (h) Song, B. Q.; Wang, X. L.; Zhang, Y. T.; Wu, X. S.; Liu, H. S.; Shao, K. Z.; Su, Z. M. *Chem. Commun.* **2015**, *51*, 9515–9518.
- (2) (a) Zhou, L.; Gao, C.; Xu, W. *ACS Appl. Mater. Interfaces* **2010**, *2*, 1483–1491. (b) Uddin, M. T.; Islam, M. A.; Mahmud, S.; Rukanuzzaman, M. *J. Hazard. Mater.* **2009**, *164*, 53–60.
- (3) (a) Crini, G. *Bioresour. Technol.* **2006**, *97*, 1061–1085. (b) Cao, M.; Lin, J.; Lü, J.; You, Y.; Liu, T.; Cao, R. *J. Hazard. Mater.* **2011**, *186*, 948. (c) Hasan, Z.; Jhung, S. H. *J. Hazard. Mater.* **2015**, *283*, 329–339. (d) Yang, Z.; Gao, S.; Li, H.; Cao, R. *J. Colloid Interface Sci.* **2012**, *375*, 172–179. (e) Lu, J.; Lin, J. X.; Zhao, X. L.; Cao, R. *Chem. Commun.* **2012**, *48*, 669–671.
- (4) (a) Yamashita, J.; Shioya, M.; Kikutani, T.; Hashimoto, T. *Carbon* **2001**, *39*, 207–214. (b) Vasanth Kumar, K.; Sivanesan, S. *J. Hazard. Mater.* **2006**, *134*, 237–244. (c) Liu, Y.; Zheng, Y.; Wang, A. *J. Environ. Sci.* **2010**, *22*, 486–493. (d) Hu, D.-D.; Lin, J.; Zhang, Q.; Lu, J.-N.; Wang, X.-Y.; Wang, Y.-W.; Bu, F.; Ding, L.-F.; Wang, L.; Wu, T. *Chem. Mater.* **2015**, *27*, 4099–4104.

- (5) (a) Zhou, H. C.; Long, J. R.; Yaghi, O. M. *Chem. Rev.* **2012**, *112*, 673–674. (b) Assen, A. H.; Belmabkhout, Y.; Adil, K.; Bhatt, P. M.; Xue, D. X.; Jiang, H.; Eddaoudi, M. *Angew. Chem., Int. Ed.* **2015**, *54*, 14353–14358. (c) Xue, D. X.; Belmabkhout, Y.; Shekhah, O.; Jiang, H.; Adil, K.; Cairns, A. J.; Eddaoudi, M. *J. Am. Chem. Soc.* **2015**, *137*, 5034–5040. (d) Wang, X. S.; Huang, Y. B.; Lin, Z. J.; Cao, R. *Dalton. Trans.* **2014**, *43*, 11950–11958. (e) Huang, Y.; Lin, Z.; Fu, H.; Wang, F.; Shen, M.; Wang, X.; Cao, R. *ChemSusChem* **2014**, *7*, 2647–2653. (f) Huang, Y.; Zhang, Y.; Chen, X.; Wu, D.; Yi, Z.; Cao, R. *Chem. Commun.* **2014**, *50*, 10115–10117. (g) Lin, Z. J.; Lu, J.; Hong, M.; Cao, R. *Chem. Soc. Rev.* **2014**, *43*, 5867–5895. (h) Wang, L. L.; Luo, F.; Dang, L. L.; Li, J. Q.; Wu, X. L.; Liu, S. J.; Luo, M. B. *J. Mater. Chem. A* **2015**, *3*, 13724–13730. (i) Jiang, Z. R.; Wang, H.; Hu, Y.; Lu, J.; Jiang, H. L. *ChemSusChem* **2015**, *8*, 878–885. (j) Jiang, H. L.; Feng, D.; Liu, T. F.; Li, J. R.; Zhou, H. C. *J. Am. Chem. Soc.* **2012**, *134*, 14690–14693.
- (6) (a) Cychosz, K. A.; Ahmad, R.; Matzger, A. J. *Chem. Sci.* **2010**, *1*, 293. (b) Han, S.; Wei, Y.; Valente, C.; Lagzi, I.; Gassensmith, J. J.; Coskun, A.; Stoddart, J. F.; Grzybowski, B. A. *J. Am. Chem. Soc.* **2010**, *132*, 16358–16361. (c) He, Y.; Tan, Y.; Zhang, J. *Huaxue Xuebao* **2014**, *72*, 1228. (d) Hu, X. L.; Liu, F. H.; Wang, H. N.; Qin, C.; Sun, C. Y.; Su, Z. M.; Liu, F. C. *J. Mater. Chem. A* **2014**, *2*, 14827–14834. (e) Jiang, H. L.; Tatsu, Y.; Lu, Z. H.; Xu, Q. *J. Am. Chem. Soc.* **2010**, *132*, 5586–5587. (f) Lan, Y. Q.; Jiang, H. L.; Li, S. L.; Xu, Q. *Adv. Mater.* **2011**, *23*, 5015–5020. (g) Zhang, X.; Gao, Y.; Liu, H.; Liu, Z. *CrystEngComm* **2015**, *17*, 6037–6043. (h) Yan, A. X.; Yao, S.; Li, Y. G.; Zhang, Z. M.; Lu, Y.; Chen, W. L.; Wang, E. B. *Chem.—Eur. J.* **2014**, *20*, 6927–6933. (i) Zhao, X.; Bu, X.; Wu, T.; Zheng, S. T.; Wang, L.; Feng, P. *Nat. Commun.* **2013**, *4*, 2344.
- (7) Sarkisov, L.; Harrison, A. *Mol. Simul.* **2011**, *37*, 1248–1257.
- (8) Dong, M. J.; Zhao, M.; Ou, S.; Zou, C.; Wu, C. D. *Angew. Chem., Int. Ed.* **2014**, *53*, 1575–1579.
- (9) Xiao, J.-D.; Qiu, L.-G.; Jiang, X.; Zhu, Y.-J.; Ye, S.; Jiang, X. *Carbon* **2013**, *59*, 372–382.
- (10) (a) Masoomi, M. Y.; Beheshti, S.; Morsali, A. *J. Mater. Chem. A* **2014**, *2*, 16863–16866. (b) Wang, Y.; Wang, L.; Liu, C.; Wang, R. *ChemCatChem* **2015**, *7*, 1559–1565. (c) Ohashi, M.; Kapoor, M. P.; Inagaki, S. *Chem. Commun.* **2008**, 841–843. (d) Tran, U. P. N.; Le, K. K. A.; Phan, N. T. S. *ACS Catal.* **2011**, *1*, 120–127.
- (11) Yi, X. C.; Huang, M. X.; Qi, Y.; Gao, E. Q. *Dalton. Trans.* **2014**, *43*, 3691–3697.